**PAPER** • **OPEN ACCESS**

# Ultrasonic assisted removal of methyl orange and bovine serum albumin from wastewater using modified activated carbons: RSM optimization and reusability

To cite this article: Imran Ahmad Khan *et al* 2024 *Mater. Res. Express* **11** 095505



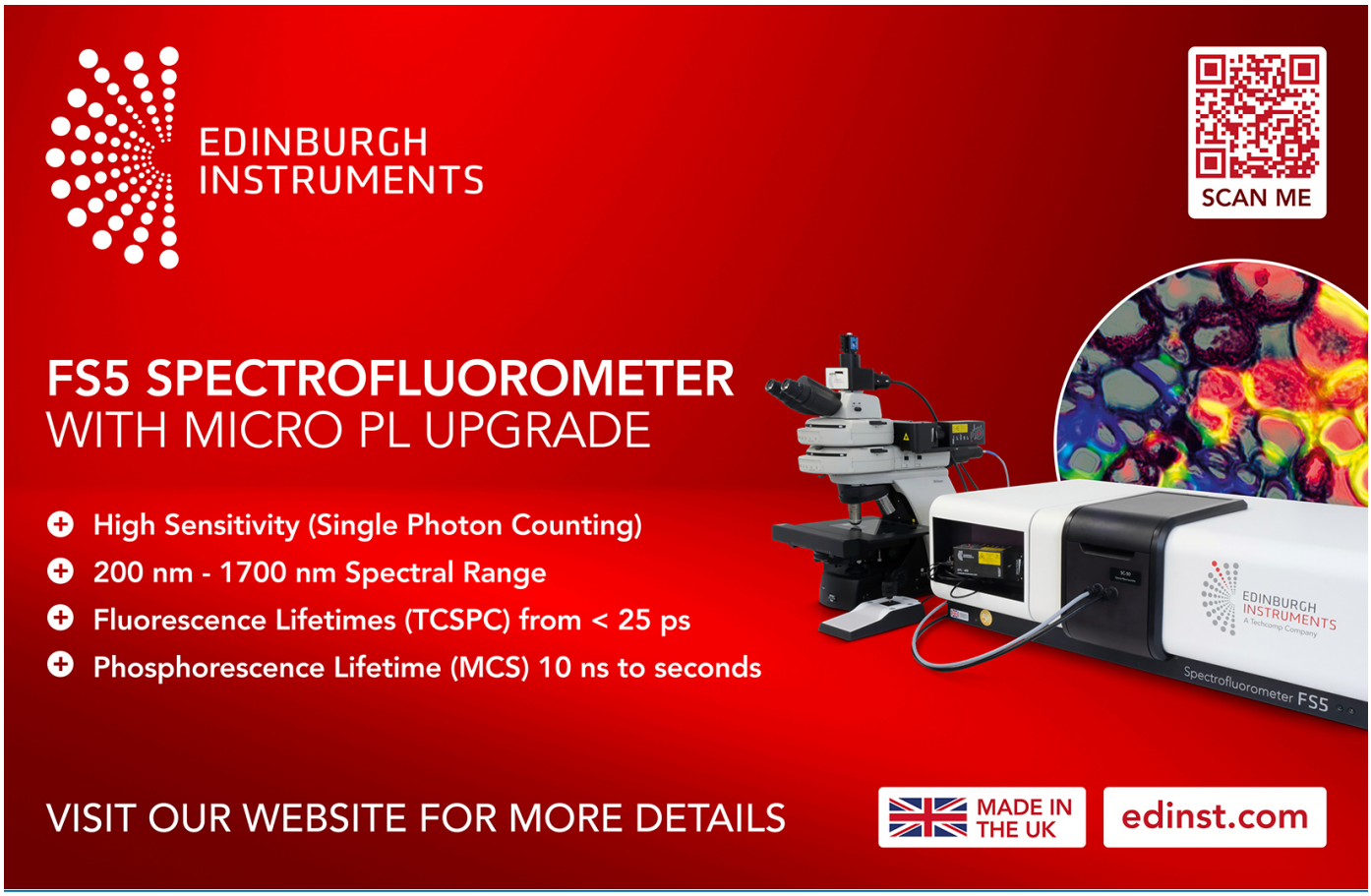

Materials Research Express

PAPER

# Ultrasonic assisted removal of methyl orange and bovine serum albumin from wastewater using modified activated carbons: RSM optimization and reusability

**Imran Ahmad Khan**[1], **Asad Ullah Khan**[1], **Kashif Mairaj Deen**[2,*], **Edouard Asselin**[2], **Rehan Sadiq**[3], **Muhammad Yasir**[4] and **Nasir M Ahmad**[1,*]

[1] School of Chemical and Materials Engineering (SCME), National University of Sciences and Technology (NUST), H-12 Sector, Islamabad 44000, Pakistan
[2] Department of Materials Engineering, The University of British Columbia, Vancouver, V6T 1Z4, BC, Canada
[3] Department of Civil Engineering, School of Engineering, University of British Columbia, Okanagan Campus, Kelowna, V1V 1V7, BC, Canada
[4] Centre of Polymer Systems, University Institute, Tomas Bata University in Zlin, Trida Tomase Bati 5678, 76001 Zlin, Czech Republic
* Authors to whom any correspondence should be addressed.

**E-mail:** kashifmairaj.deen@ubc.ca **and** nasir.ahmad@scme.nust.edu.pk

**Keywords:** activated carbon, adsorption isotherms, water treatment, dye removal

Supplementary material for this article is available online

OPEN ACCESS

RECEIVED
16 June 2024

REVISED
26 August 2024

ACCEPTED FOR PUBLICATION
3 September 2024

PUBLISHED
13 September 2024



## Abstract

The removal of industrial pollutants from water remains a significant challenge in water treatment processes. This study investigated the efficacy of powder-activated carbon (PAC), thermally modified PAC (TPAC), and chemically modified PAC (CPAC) for removing bovine serum albumin (BSA) and methyl orange (MO) from simulated wastewater. After undergoing treatment, the BET surface area of TPAC increased to 823 $m^2 g^{-1}$, while that of CPAC increased to 657 $m^2 g^{-1}$ compared to the initial surface area of pristine PAC, which was 619 $m^2 g^{-1}$. Batch adsorption experiments assisted by ultrasonication were conducted to evaluate the impact of solution pH, initial concentration, and contact time on the adsorption capacities ($q_{max}$) of BSA and MO. TPAC demonstrated superior performance, achieving $q_{max}$ values of 152 mg $g^{-1}$ for MO and 133 mg $g^{-1}$ for BSA, compared to PAC, which provided $q_{max}$ values of 124 mg $g^{-1}$ and 112 mg $g^{-1}$, respectively. Furthermore, pH levels of 3 and 5 were identified as highly effective for the removal of MO and BSA from water, respectively. The adsorption kinetics of both MO and BSA followed pseudo2nd-order ($R^2 > 0.99$) reaction kinetics under both batch and ultrasonic conditions, confirming the removal of contaminants through chemisorption. The adsorption trends also satisfied the Langmuir isothermal model, indicating the formation of a uniform monolayer during the adsorption process of these contaminants. To understand the simultaneous effect of all the variables, response surface methodology (RSM) using central composite design (CCD) was used to predict the adsorption capacities of CPAC. After five adsorption cycles, the removal efficiencies of MO (from 98% to 80%) and BSA (from 55% to 40%) decreased in the CPAC system. The results suggested that CPAC can be effectively utilized to remove MO from wastewater.

## 1. Introduction

Environmental water pollution has always been a persistent and significant challenge, affecting both industrial progress and public health (Liu *et al* 2019). Various industrial sectors, including textiles, pharmaceuticals, and chemicals, are major sources of water pollution since they use high levels of water and chemicals for processing. For instance, the textile industry uses dyes for coloring and bovine serum albumin (BSA) as a textile coating (Ohashi *et al* 2012, Sk and Aal 2020). These pollutants in water are difficult to degrade because of their complex structure and xenobiotic characteristics (Naushad *et al* 2019, Sakamoto *et al* 2019). Organic dyes such as methyl

orange (MO) are nondegradable when released in industrial effluents and pose a major threat to the environment. Such organic-textile effluents may cause dermatitis, eye infection, cancer, and cell mutations and may adversely affect aquatic life (Sivarajasekar and Baskar 2014, Lellis *et al* 2019). Another emerging pollutant of biological origin, BSA, is a globular protein that accounts for ~55% of the overall plasma protein content (Szymaszek *et al* 2022). BSA is used in the textile sector as an adhesive for immobilizing coatings on the surface of the fabric as well as a sorbent for azo dyes (MO), which are generally resistant to biodegradation (Ohashi *et al* 2012, Wang *et al* 2018). BSA in effluent water must be removed before being released into natural water streams (Tang *et al* 2019). It is vital to remove BSA and other dye compounds from wastewater due to their deleterious effects on aquatic and human life (Bayer 2010). There are several methods for removing dyes and phenolic compounds from water, including adsorption, membrane technology, ozonation, biodegradation, and photocatalysis (Beker *et al* 2010, Jiang *et al* 2015, Lima *et al* 2021).

Membrane filtration effectively removes all dye types with high stability, efficiency, compactness, and environmental friendliness, but suffers from fouling (Gholami Derami *et al* 2020, Bal and Thakur 2021). Ozonation is highly reactive and efficient but lacks control (Muniyasamy *et al* 2020, Bal and Thakur 2021). Biosorption/biodegradation is cost-effective but slow and difficult to optimize (M-Ridha *et al* 2020). Photocatalysis, such as Ba-doped g-C3N4 achieving 91.94% tetracycline degradation in 120 min, is effective but can produce toxic byproducts (Bui *et al* 2020, Moosavi *et al* 2020).

Adsorption is effective due to its simple operational design, reusability, high efficiency, cost-effectiveness, and low waste generation (Jawad and Abdulhameed 2020). In comparison to conventional adsorption techniques, sonication-aided methods are expected to enhance the adsorption efficiency due to the increased solute mass transfer by acoustic waves (Hamdaoui and Naffrechoux 2009). Many types of adsorbents have been used for this purpose, but AC is considered an effective adsorbent for the removal of organic chemicals due to its superior adsorption capabilities (Ma *et al* 2013). Previous studies have demonstrated that AC is an economical and effective adsorbent material on a large scale. It has also been reported that PAC has a greater adsorption efficiency for many organic compounds than granular-activated carbon (GAC) due to its greater surface area and porosity (Vukčević *et al* 2004). The adsorption of textile dyes on AC in a batch process is an endothermic process, indicating that dye molecules require energy to penetrate through the microporous structure of AC (Al-Degs *et al* 2008).

The contaminant removal efficiency of AC is highly influenced by its surface chemistry. Consequently, surface modification with different functional groups (−OH, −COOH, and −NH) plays a crucial role in tailoring AC materials for specific applications (Belayachi *et al* 2016, Shafeeyan *et al* 2010). A study investigated the chemical surface modification response of AC produced from Elaeagnus waste and chemically activated with $ZnCl_2$ to attain suitable surface characteristics for the adsorption of BSA and revealed that the adsorption yield decreased due to an increase in temperature and initial concentration of BSA (Geçgel and Üner 2018). Interestingly, the combination of factors such as ultrasonication and stirring significantly improved the removal of organic contaminants from wastewater by AC (Landi *et al* 2010).

Various studies have explored the modification of AC for enhanced adsorption of contaminants, though key comparisons and regeneration analyses are often lacking. Estrada *et al* (2021) investigated MO adsorption using chemically modified magnetic AC with different AC ratios, finding the highest capacity at a 2:1 ratio, but they did not assess regeneration or compare with physically activated carbon. El-Bindary *et al* (2022) used KOH to chemically activate AC, achieving a 91 mg $g^{-1}$ adsorption capacity for malachite green, while Bekhoukh *et al* (2022) synthesized a novel AC-polyaniline composite that showed a high initial MO removal capacity of 192.52 mg $g^{-1}$ but significantly declined upon regeneration. Alharbi *et al* (2023) modified AC through hydrothermal carbonization and microwave-assisted $H_3PO_4$ activation, achieving optimal Remazol Brilliant Blue R removal at pH 3, though with slow equilibrium times. El-Bery *et al* (2022) reported that increasing activation temperature enhanced surface area but noted a decline in phenol removal efficiency after multiple regeneration cycles. Lastly, Bumajdad and Hasila (2023) synthesized N-doped ACs using metal carbonate activators, achieving over 99.9% removal of Cr(VI) and Pb(II), though optimal adsorption was at low adsorbate concentrations, and no regeneration study was conducted. These studies demonstrate varied methods of AC modification but lack direct comparisons between physical and chemical modifications, as well as consistent evaluations of regeneration and multi-contaminant removal.

The enhancement of dye removal from wastewater using AC is influenced not only by surface modification but also by factors such as ultrasonication and contact time, as demonstrated by Landi *et al* (2010). Typically, these factors are studied using the one-factor-at-a-time (OFAT) approach, which, as Madondo and Chetty (2022) pointed out, fails to capture the interaction effects between multiple variables. The use of RSM could address this gap by optimizing multifactor systems with fewer experiments, as shown by Yang *et al* (2022). While RSM has been applied to optimize conditions for MO removal by nonfunctionalized AC in batch processes (Danish *et al* 2014, Rondina *et al* 2019), no studies have explored the combined effect of ultrasonication parameters on the removal of both BSA protein and MO dye using modified AC. To fill this gap, this study

optimized the ultrasonication-assisted adsorption process for these contaminants and validated the results experimentally. Previous studies have shown that chemical oxidative treatments (Foo and Hameed 2010) and alkaline treatments (Foo and Hameed 2012, Liu *et al* 2016, Bonyadi *et al* 2019) effectively enhance AC's pollutant removal capabilities, but these studies focused on a single functionalization method tailored to specific pollutants. This study advances the field by systematically investigating both chemical and physical functionalization of AC for the simultaneous removal of diverse pollutants, including textile dyes and BSA protein. Comparative studies have reported relatively low adsorption capacities for existing materials, such as nano-activated carbon (28 mg $g^{-1}$) with a 90 min equilibrium time (Shokry *et al* 2019), commercial granular AC (3.32 mg $g^{-1}$) for azo dyes, and orange peel-derived AC with a capacity of 33–38 mg $g^{-1}$ (Khader *et al* 2021, Ramutshatsha-Makhwedzha *et al* 2022). For BSA removal, titanium dioxide (42.6 mg $g^{-1}$) and hydroxyapatite (28 mg $g^{-1}$) require up to 48 h to reach equilibrium (Kopac *et al* 2008, Swain and Sarkar 2013). To address the limitations of low adsorption capacity, this study developed two AC materials: one through thermal treatment to increased surface area and porosity, and the other via chemical modification with aminopropyltrimethoxysilane (APTMS) to introduce functional groups that enhance selectivity and adsorption capacity for target contaminants. While other materials like zeolites (Hamd *et al* 2023) and metal–organic frameworks (Mohammadi *et al* 2022) offer high selectivity, they are often more costly and may lack the thermal and chemical stability of activated carbon, underscoring the practical advantages of the functionalized AC developed in this study.

This research focuses on using RSM to model and predict the key parameters influencing the adsorption of BSA and MO onto thermally and chemically modified PAC. By combining thermal and chemical modification techniques—thermal treatment to enhance surface area and pore volume, and chemical modification with APTMS to introduce functional groups—the study aims to significantly improve the adsorption capacity and selectivity of PAC for these contaminants. The novelty of this work lies in the systematic investigation of both thermal and chemical modifications alongside the application of ultrasonication to optimize the adsorption process, something not previously reported for these specific contaminants. Adsorption isotherms and kinetic models were employed to elucidate the adsorption mechanisms, while RSM was used to optimize ultrasonication parameters, including sonication time, analyte concentration, and pH, to maximize removal efficiency. The feasibility of the modified PAC for reuse was assessed over five consecutive cycles, with results compared against existing materials in the literature. This research offers valuable insights and guidelines for designing efficient adsorption systems for the removal of organic pollutants from industrial wastewater, highlighting the complementary benefits of thermal and chemical modifications.

## 2. Materials and methods

The PAC was purchased from Merck & Co. (Germany). Analytical grade reagents, i.e., (3-aminopropyl) trimethoxysilane (97%) (Sigma-Aldrich), BSA protein (B005) (CAISSON Laboratories, Inc. Smithfield, Utah, USA), and MO from Sigma Aldrich (St. Louis, USA), were used as received without further purification.

### 2.1. Chemical functionalization of the PAC

A flow diagram of the experimental process is shown in figure 1(a), whereas the chemical modification steps of the PAC sample are shown in figure 1(b). For chemical oxidation, 5 g of PAC was treated with 50 ml of $HNO_3$ (20%) at 80 °C and refluxed for 3 h. The chemically oxidized PAC was washed with deionized (DI) water and dried at 105 °C. The dried PAC was added to 100 ml of toluene and 1 ml of (3aminopropyl) trimethoxysilane (designated APTMS) under continuous magnetic stirring for 24 h at 250 rpm. The APTMS-PAC was further washed with toluene and acetone, followed by vacuum drying at 60 °C for 4 h. This chemical modification resulted in surface functionalization of the PAC. The functionalized PAC (designated CPAC) was stored in a closed container under dry conditions for further use.

### 2.2. Thermal modification of the PAC

Prior to thermal treatment, the PAC specimen was immersed and rinsed in deionized water for 24 h, followed by drying in a vacuum oven at 110 °C. PAC was then introduced into a ceramic dish, which was then positioned in a box furnace (MS-1600) set at a temperature of 900 °C for 1 h, maintaining a controlled atmosphere with flowing nitrogen gas to limit oxidation of the PAC sample. The resulting heat-treated activated carbon is referred to as TPAC in the subsequent discourse.

### 2.3. Characterization of AC-based samples

*An* ATRFTIR Bruker ALPHA spectrophotometer (Germany) was used to evaluate the surface functionality of the modified PAC samples. The range was set between 600 and 4000 $cm^{-1,}$ and the resolution was 4 $cm^{-1}$. The

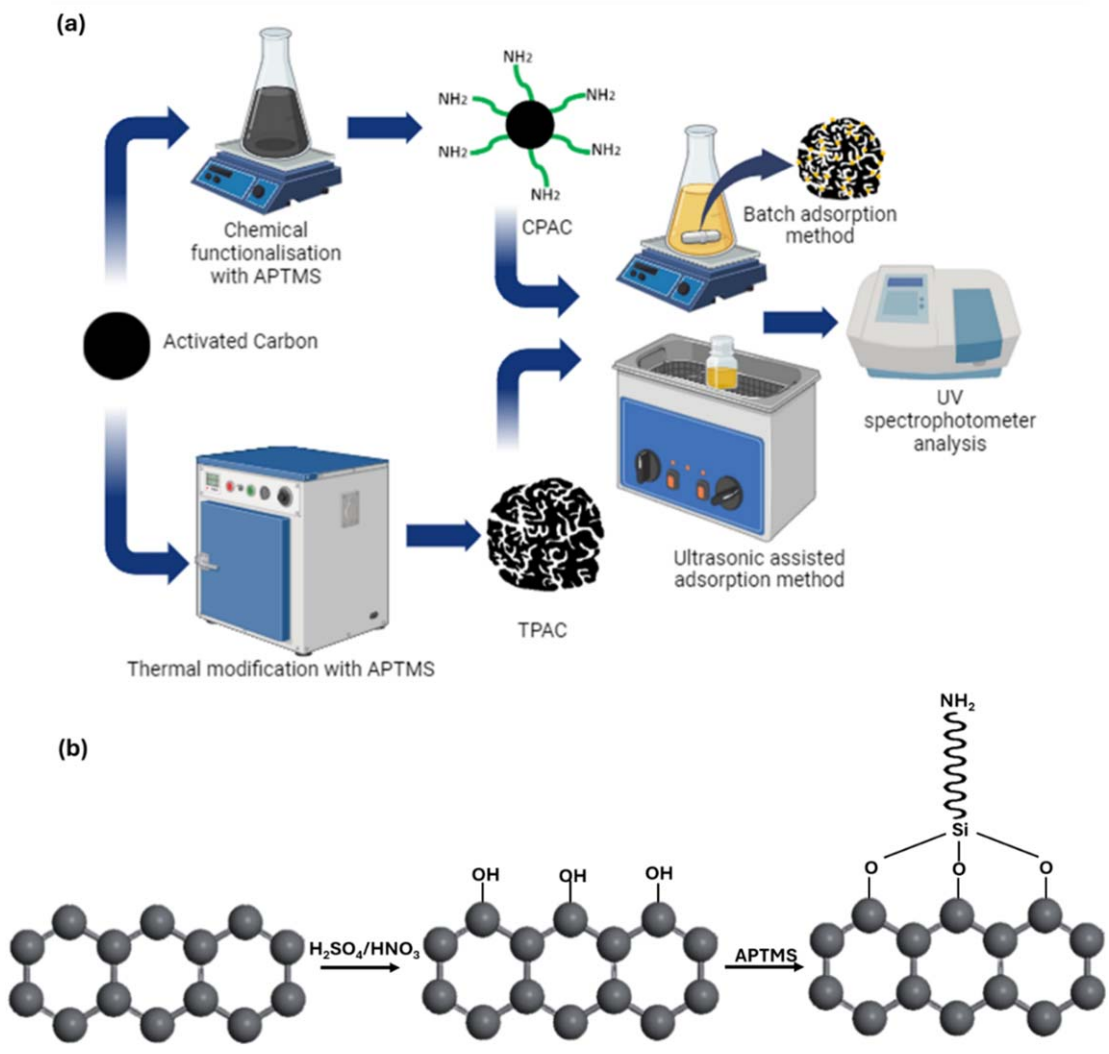


**Figure 1.** (a) A schematic flow sheet diagram showing the steps of PAC surface modification and (b) the functionalization process of PAC via chemical modification.

surface morphology of the modified PAC samples was studied by scanning electron microscopy (SEM) (JEOL JSM 6490 A, Japan) at an accelerating voltage of 10 kV. The adsorption capacity and concentration of the contaminants in the treated sample were measured using a PerkinElmer Lambda 365 UV/VIS spectrophotometer (USA). The surface areas and pore sizes of the PAC and functionalized PAC samples were determined using the Brunauer–Emmett–Teller (BET) adsorption technique with $N_2$ (at 77 K) on an ASAP 2420 system (Micromeritics, USA).

### 2.4. Adsorption studies and analytical procedure

Organic species, i.e., BSA and MO, were separately added to DI water and diluted to the desired concentrations of typically 30, 60, or 90 ppm. Known amounts TPAC or CPAC were added to these simulated waste solutions in separate batches, i.e., agitated at 50 rpm using a hotplate (SCILOGEX (MS7H550S)) and sonicated (Ultrasonic bath sonicator Cole-Parmer®) at an operating frequency of 42 kHz for various time intervals of 15, 30, 45, 60 and 120 min. After refluxing with these PAC samples, a representative sample of each solution containing a known initial concentration of organic species ($C_i$) was collected at regular intervals. A nylon syringe filter (0.45 μm) was used to filter the solutions, and the filtrate solution was then immediately tested in a PerkinElmer Lambda 365 UV/VIS spectrophotometer in the range of 200–800 nm. The UV/VIS absorbance intensity was measured, and by using the Beer–Lambert law, the % adsorption ($R$) and equilibrium adsorption capacity ($q_e$) of the PAC samples were calculated according to equations (1) and (2), respectively.

$$R = \frac{(C_i - C_t)}{C_i} \times 100 \quad (1)$$

where $C_i$ (mg/l) is the initial concentration of either BSA or MO, and $C_t$ (mg/L) is the concentration after time (t).

$$q_e = \frac{(C_i - C_e)V}{m} \tag{2}$$

where $C_e$ (mg/L) is the equilibrium concentration of organic species, $V$ (L) is the adsorbate solution volume, and $m$ (g) is the mass of adsorbed species. To construct the adsorption isotherms, the $C_i$ values of the organic pollutants were varied to 30, 60, and 90 ppm.

The central composite design (CCD) model was applied using Design-Expert software v13.0 to estimate and optimize the key factors (pH, time, and pollutant concentration) and their interaction effects on the removal of MO and BSA by functionalized CPAC. This CCD model incorporates factorial points, including axial and central points, to comprehensively explore all the parameters (Yasir *et al* 2022). The investigated levels of the primary factors are provided in table S1.

A second-order polynomial equation, expressed by equation (3), was used to model the relationship between the independent factors and the obtained responses.

$$Y = \beta_0 + \sum_{i=1}^{k} \beta_i X_i + \sum_{i=1}^{k} \beta_{ii} X_i^2 \sum_{i=1}^{k}. \sum_{j=i+1}^{k} \beta_{ij} X_i X_j + e \tag{3}$$

where $Y$ is the response (removal efficiency of MO or BSA); $X_i$ and $X_{ij}$ are the encoded parameters; and $\beta_0$, $\beta_i$, $\beta_{ii}$, and $\beta_{ij}$ are the linear, quadratic, and interaction coefficients, respectively. The desirability function is then utilized to determine the optimal levels for each investigated parameter based on the generated results.

### 2.5. Reusability

Given the significance of economic considerations, it is important to evaluate the potential for reusing adsorbent materials. We conducted desorption experiments to measure the extent to which CPAC can be reused. For this purpose, CPAC containing MO and BSA was subjected to desorption using a 0.1 M NaOH solution for 60 min, corresponding to the time at which adsorption equilibrium was reached. The CPAC was then repeatedly rinsed with deionized water until it reached a neutral pH; afterward, it was dried and subsequently reused for adsorption purposes (Lekene *et al* 2021).

### 2.6. Statistical analysis

The data are presented as the mean ± standard error. Statistical analysis was conducted using Design Expert software v.13.0, and the data were plotted with OriginLab Pro v.9.0. The difference between values was assessed through one-way analysis of variance (ANOVA), with a significance level set at $p < 0.05$. Error analysis metrics, including the determination coefficient ($R^2$), were employed to evaluate differences between the experimental and theoretical data.

## 3. Results and discussion

### 3.1. Characterization analysis

*3.1.1. Surface area measurements and ATR-FTIR analysis of the PAC samples*

The PAC had a BET surface area of 619 $m^2\,g^{-1}$, whereas TPAC was 823 $m^2\,g^{-1}$ and CPAC was 657 $m^2\,g^{-1}$ (Table S2). Heat treatment at high temperatures significantly enhanced the surface area and structure of the PAC, consistent with previous literature findings (Attia *et al* 2006). For TPAC samples, the heat treatment induced the formation of new pores, as evidenced by SEM analysis. This increase in surface area enhances adsorption capacity by generating additional surface-active sites (Adam *et al* 2015a). In contrast, chemical surface functionalization of the AC reduced the surface area. This reduction is due to interactions between surface active sites and APTMS, which block effective adsorption sites and obstruct the internal pore structure, thereby decreasing the available surface area for adsorption (Ünveren *et al* 2017a).

Figure. S1 *(Supplementary Information)* shows the ATR-FTIR spectra of the PAC, TPAC, and CPAC samples. Similar FTIR spectra for both the PAC and TPAC indicated that high-temperature heat treatment did not affect the surface composition of the PAC (Mines *et al* 2017). The peaks at 3383.2 $cm^{-1}$ and 2800–3000 $cm^{-1}$ are associated with the presence of an amine group on the surface of CPAC, specifically referring to the stretching of -NH bonds (Abbas *et al* 2020). The presence of weak stretching bands at 1653 $cm^{-1}$ and 1028 $cm^{-1}$ in the FTIR spectrum reflects the carboxylic (C=O) functional group and the Si–O–Si bridge. Additionally, the in-plane and out-of-plane deformed -OH groups of the carboxylic acid were evident in the spectrum from the peaks at 1464 and 938 $cm^{-1}$, respectively, which are consistent with the literature (Nifas and Forteza 2019).

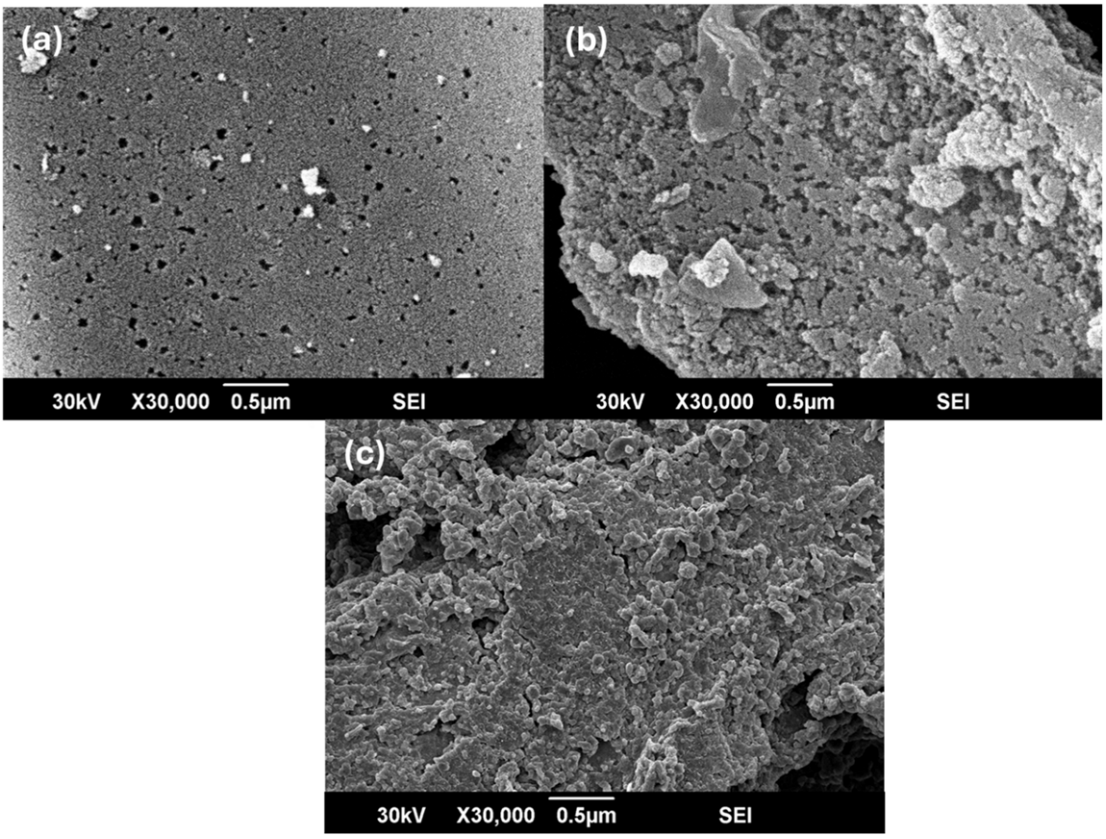


**Figure 2.** Surface morphology of (a) PAC, (b) TPAC, and (c) CPAC samples.

*3.1.2. Surface morphology and point of zero charge*

The surface morphology of the PAC, TPAC, and CPAC samples was examined by SEM at 30,000X magnification, as shown in figure 2. The surface of the PAC was found to be smooth, containing a very fine porous structure (figure 2(a)). The TPAC sample is shown in figure 2(b), which also revealed a highly dense porous structure because of high-temperature treatment in a controlled environment. The formation of a more porous structure in the TPAC sample facilitates the adsorption of MO and BSA pollutants from wastewater (Lütke *et al* 2019). The apparent increase in the pore size (31.4 Å) also indicates an increase in the surface roughness of the TPAC sample. On the other hand, the absence of a porous structure and relatively low surface roughness of the CPAC samples resulted from a possible blockage of the pores during the functionalization process, which can lead to a decrease in adsorption (figure 2(c)) (Meng *et al* 2009).

For the TPAC samples, the heat treatment process leads to the formation of new pores, as confirmed by the SEM images. This treatment significantly increases the surface area of AC by expanding the existing pore network and generation of new pores. In contrast, the CPAC samples have a surface resembling a coated structure with a shiny appearance. This is attributed to the presence of APTMS, which fills or blocks the pores (Ünveren *et al* 2017b). The introduction of APTMS, while beneficial for functionalization, can obstruct the internal pore structure, leading to a decrease in available surface area for adsorption.

The point of zero charge (PZC) for PAC, TPAC, and CPAC was determined using the drift method. A 0.01 M NaCl solution was prepared and purged with nitrogen to remove dissolved oxygen and carbon dioxide. A total 50 ml of this solution was added into a series of 100 ml beakers, and the pH was adjusted from 3 to 11 using HCl and NaOH. In each beaker, 150 mg of the adsorbents (AC samples) was added, and the suspensions were stirred for 48 h at 250 rpm. Following this, the suspensions were filtered, and the final pH of the solution was measured. The difference in pH (ΔpH) between the final pH and the initial pH (pHi) was plotted against pHi. The point where ΔpH equaled zero was identified as the PZC (Ntakirutimana *et al* 2019).

The PZC values were found to be 6.5 for PAC, 6.6 for TPAC, and 8.2 for CPAC as shown in figure 3. The close similarity in PZC values between PAC and TPAC suggests that thermal treatment did not significantly alter the chemical structure of AC. In contrast, the higher PZC of CPAC, which shifted to a more alkaline pH, indicates that amine functionalization of CPAC influences its surface charge properties, attributed to the presence of amine groups after functionalization (Lekene *et al* 2021).

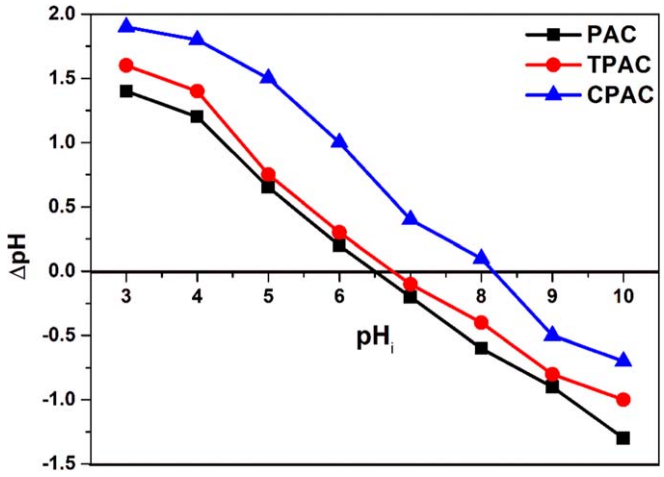


**Figure 3.** Point of zero charge measurement plots of (a) PAC, (b) TPAC, and (c) CPAC obtained via drift method.

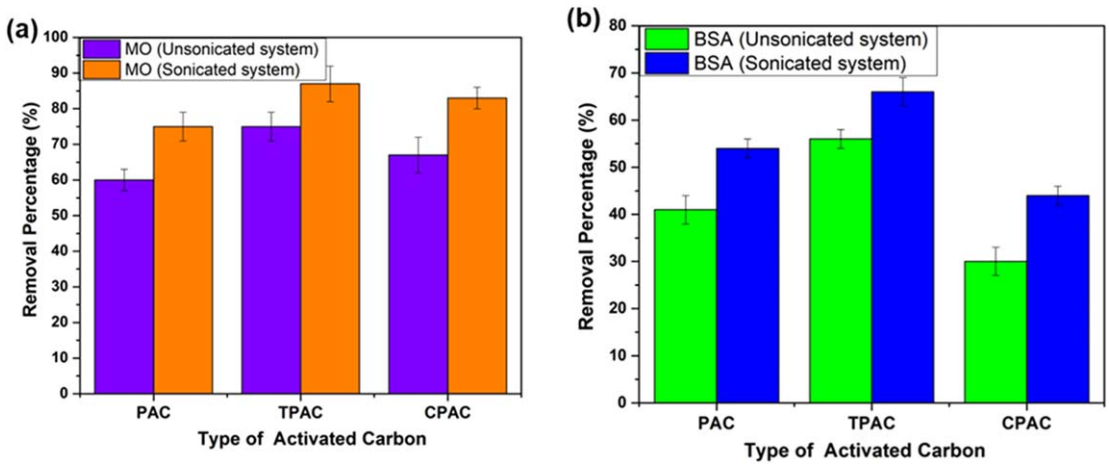


**Figure 4.** Removal of (a) MO and (b) BSA from solution by PAC, TPAC, and CPAC during conventional batch adsorption and ultrasound-assisted batch adsorption processes. (Conditions: pH = 7, dosage = 0.05 g, MO and BSA concentration = 90 ppm, time = 60 min).

### 3.2. Adsorption analysis

*3.2.1. Effect of modification treatment and ultrasonication on the adsorption of MO and BSA*

For preliminary evaluation, the removal of organic contaminants from the simulated wastewater, i.e., BSA and MO, was investigated both in batch and sonication adsorption processes. The removal efficiency of the MO dye and BSA by these PAC samples followed the descending order of TPAC > CPAC > PAC (which corresponds well to their surface area and pore volume), as shown in figures 4(a) and (b), respectively. For instance, compared to PAC and CPAC, the large removal rate of MO by TPAC both in the batch and sonication processes is attributed to its larger specific surface area (table S2), indicating a larger number of active sites for contaminant adsorption (Sáenz-Alanís *et al* 2017). The increased surface area and pore density after thermal treatment of the PAC were also evident via SEM (figure 4(b)). The CPAC sample, even though it has a lower surface area than the TPAC sample, still demonstrated comparable adsorption of MO. Chemical modification introduced nitrogen-containing functional groups on the surface of PAC, which increased the availability of delocalized electrons in the PAC structure for p-p interactions with the MO molecular structure (Naushad *et al* 2019). The adsorption of BSA on CPAC samples was found to be 30% (unsonicated system), which can be explained by the presence of $-NH_2$ surface functional groups, which could hinder the attachment of the protein to its surface due to electrostatic repulsion (Adamczyk *et al* 2018).

Figure 4 also shows an increase in the adsorption rate of the organic contaminants and removal efficiency during exposure to PAC samples under continuous sonication (Ma *et al* 2012). For instance, with sonication, the removal efficiency of MO by CPAC was found to be 83% compared to that of the batch process, which exhibited 67% removal efficiency. Compared to the batch absorption process, continuous sonication offers an

approximately 17% increase in the removal efficiency of both organic contaminants, which is attributed to shock-wave-induced micro-stirring of the solution driving adsorbed species into the porous PAC structure (Abid *et al* 2022). During sonication, symmetric (within the liquid phase) and asymmetric (at the solid–liquid interface) shock waves are generated. The collapse of air bubbles and turbulent flow of the dissolved species at the solid–liquid interface enhance the mass transfer rate within the porous structure. Moreover, ultrasonication increases the intensity of dissolved contaminant mass transfer across the boundary layer and into the pores, which improves adsorption, as demonstrated in the experimental results (figure 4) (Nifas and Forteza 2019).

*3.2.2. Effect of pH and adsorption mechanism*

Compared to PAC and TPAC, the adsorption of MO by CPAC is substantially affected by the pH of the solution due to the presence of -$NH_2$ functional groups. Figure S2(a), (b) (*Supplementary Information*) shows the MO adsorption behavior of these materials across the pH range of 3.0–11.0. The removal efficiency of MO over PAC and TPAC remained independent of the solution pH. However, the MO removal efficiency of the CPAC decreased with increasing pH from 3.0 to 11.0. This decrease in the adsorption efficiency is possibly associated with the electrostatic repulsion between the surface functionality of the CPAC and MO molecules. The –$NH_2$ functional group on the CPAC generated a positive surface charge in acidic media through the protonation of the amino group (Huang *et al* 2015). Consequently, the negatively charged anionic dye MO may adsorb via electrostatic attraction, as illustrated in figure S3(a). As the solution pH increased, the reduction in $H^+$ activity resulted in decreased protonation of the amino groups, causing the surface of the CPAC to become negatively charged, thereby leading to a decrease in MO adsorption over CPAC. Hence, it is proposed that strong ionic interactions primarily govern the adsorption of MO on CPAC, making it particularly suitable under acidic conditions. The effect of pH on BSA adsorption over PAC samples was also studied, as shown in figure S2(c)–(d). The maximum adsorption occurred in solutions with a pH of 5 because proteins exhibit a relatively stable structure and possess a net zero charge at the isoelectric point (for BSA, this range is typically between 4.5 and 5.0). Under these conditions, biomolecules are more active and maintain their three-dimensional structure. However, persistent pH levels below or above the isoelectric threshold can cause these structures to break down, adversely affecting the quantity of adsorption. Positive charges are often present at pH levels below the isoelectric point of BSA, while an overall negative charge typically exists at pH levels above it (Çalımlı *et al* 2019). As a result, at pH 3.0 (pH $<$ pI SE), there is stronger repulsion between the positively charged BSA and protonated –$NH_2$ functional groups of CPAC (Figure S3), leading to minimal adsorption, as observed in figure S2(c)–(d). In comparison, TPAC demonstrated a maximum adsorption capacity of approximately 60%, which increased to 72% under ultrasonication at pH 5. Overall, at all pH levels, the application of ultrasonication improved the removal efficiency of both MO and BSA over that of the PAC, TPAC and CPAC samples.

*3.2.3. Effect of contact time*

The effect of the adsorption behavior of PAC, TPAC, and CPAC on the removal of BSA and MO pollutants as a function of exposure time is shown in figure 5. During the initial 30 min , a rapid increase in removal was attributed to the availability of a large number of active sites on the surface of all AC samples (Ma *et al* 2013, Panda *et al* 2017). As the exposure time progresses, these sites become filled, leading to the saturation of active sites due to the adsorption of organic contaminants, as indicated by the plateau in the adsorption curves (after 60 min of exposure as shown in figures 5(a)–(c). Overall, ultrasonication had a positive impact on the removal of both BSA and MO by all the PAC, TPAC, and CPAC samples compared to conventional batch adsorption processes. However, TPAC had the highest removal efficiencies for BSA and MO (approximately 70% and 95%, respectively) within an hour. Additionally, figure 5(d) illustrates the preparation of stock solutions of methyl orange for establishing a calibration curve for UV–visible spectra. Figures 5(e), (g), (h) shows the filtrate collected after refluxing methyl orange solutions with powdered activated carbon (PAC) at initial concentrations ($C_i$) of 30 ppm, 60 ppm and 90 ppm.

*3.2.4. Effect of initial concentration of the organic contaminants*

The effect of the initial concentrations of BSA and MO on the maximum adsorption capacity ($q_{max}$) of PAC, TPAC, and CPAC was calculated based on the initial and final concentrations of contaminants after the adsorption study, as shown in figure 6. Briefly, PAC is generally used during the tertiary stage of wastewater stream treatment in a textile effluent treatment plant. During this stage, the target is to remove residual contaminants from the primary and secondary treatment stages. Therefore, the low concentrations of these species are expected (ranging from 10–100 ppm). As a result, tertiary treatment stage ensures that nearly 99% of the overall contaminant concentration in the wastewater is eliminated. Based on this, the initial concentrations of the organic contaminants (i.e. MO and BSA) were varied from 30 to 90 ppm. The $q_{max}$ of each sample was directly associated with the initial concentration of BSA and MO in the solution (Panda *et al* 2017). Initially, the large availability of active sites on the AC samples promoted rapid adsorption of contaminants from the

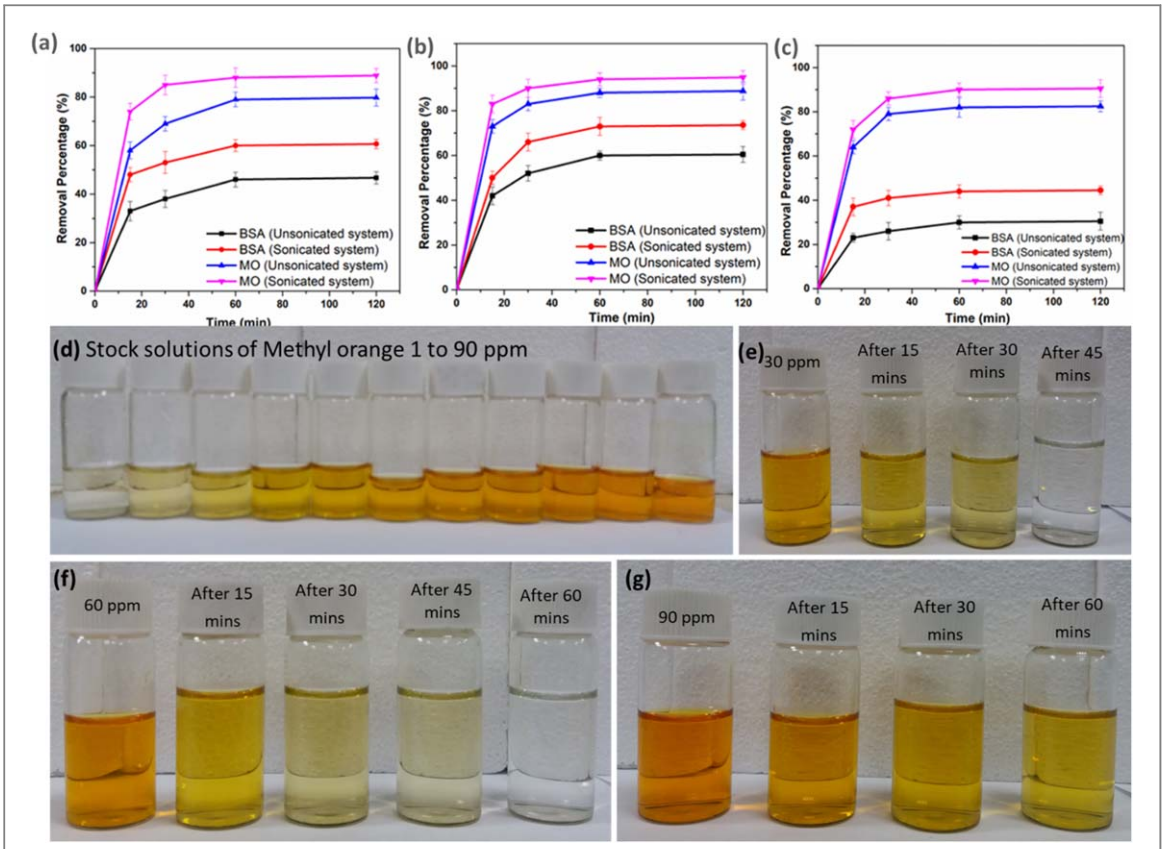


**Figure 5.** The removal of BSA and MO with (a) PAC, (b) TPAC, and (c) CPAC as a function of exposure time during conventional batch adsorption and ultrasonication-assisted batch adsorption processes (conditions: pH = 7, dosage = 0.05 g, MO and BSA concentration = 60 ppm), (d) stock solutions of MO, (e) filtrate samples of MO solutions with a PAC concentration of 30 ppm, (f) 60 ppm, and g) 90 ppm.

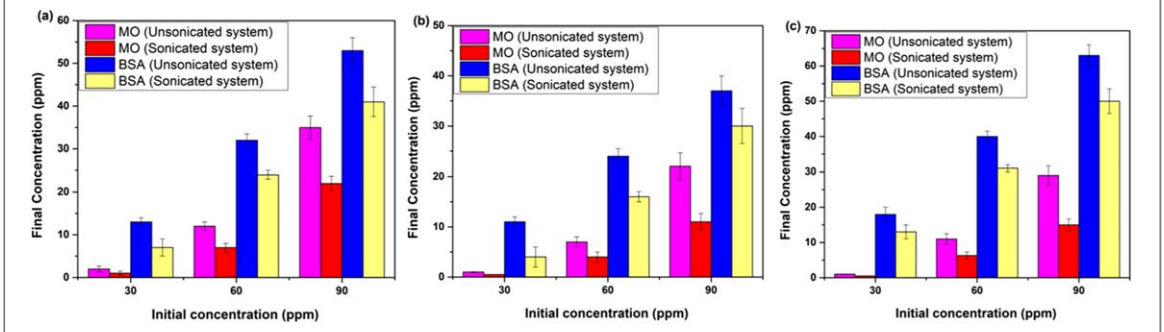


**Figure 6.** Effect of initial concentration of BSA and MO on the adsorption of (a) PAC, (b) TPAC, and (c) CPAC. (Conditions: pH = 7, dosage = 0.05 g, time = 60 min).

solution, followed by the prevalence of mass transfer limitations over time. A low initial pollutant concentration leads to higher efficiency due to the greater number of available sites. However, in the case of high initial pollutant concentrations, relatively lower efficiency is achieved due to the excess pollutant concentration and limited surface area of AC-based adsorbents (Srivastava *et al* 2006). TPAC had greater adsorption of MO than did BSA at neutral pH, as indicated by the significantly lower final concentrations. Similarly, the removal of contaminants increased rapidly under applied ultrasonication, as evidenced by the low final concentration of each contaminant compared to that of the conventional batch adsorption process.

### 3.3. Adsorption kinetics

To study the adsorption mechanism of PAC, TPAC, and CPAC for organic contaminants, pseudo-first-order (equation (4)) (Qiu *et al* 2009) and pseudo-second-order (equation (5)) kinetic models (Ho 2006) were applied to the experimental data.

$$\ln(q_e - q_t) = \ln q_e - k_1 t \tag{4}$$

$$\frac{t}{q_t} = \frac{1}{k_2 q_e^2} + \frac{t}{q_e} \tag{5}$$

where $q_e$ (mg/g) is the adsorbent capacity at equilibrium, $q_t$ (mg/g) is the adsorbent capacity at time t (min), and $k_1$ ($min^{-1}$) is the adsorption rate constant. The value of $k_1$ (at 25 °C) in equation (4) can be calculated by plotting $ln(q_e—q_t)$ vs $t$, as shown in figures S4(a), (c). Additionally, the second-order adsorption rate constant, $k_2$ (g/mg. min), was determined by linear fitting of $t/q_t$ versus $t$, as shown in figures S4(b), (d).

The adsorption kinetics of both the organic contaminants (MO and BSA) under both batch and ultrasonication-assisted adsorption conditions conformed to pseudo 2nd-order reaction kinetics, as shown in figures S4(b), (d). The adsorption kinetics of BSA and MO for PAC, TPAC, and CPAC were attributed to a 2nd-order reaction with a high fitting regression coefficient ($R^2 > 0.99$). Additionally, the $q_{e,cal}$ values obtained were found to strongly agree with the $q_{e,exp}$ values, as given in table S3 *(Supplementary Information)*. Moreover, a significant difference in the $q_{e,cal}$ and $q_{e,exp}$ values overruled the first-order reaction kinetics for all samples for both pollutants under sonicated and unsonicated batch conditions. These results suggest that the organic contaminants would be chemisorbed on the AC-based samples independently of the application of ultrasonication. These results are supported by the reported literature showing similar behavior of AC-based adsorbents following second-order adsorption kinetics for the removal of organic contaminants (Sáenz-Alanís *et al* 2017). The chemosorption of BSA and MO on these PAC samples was related to the overlap of the p-electrons in the aromatic rings ($sp^2$ orbitals) of the organic contaminants with the delocalized electrons on the surface of AC (De La Luz-Asunción *et al* 2015). The presence of nitrogen-containing functional groups on the surface of the CPAC sample ensured a high electron density, which could facilitate dominant p-p dispersive interactions during exposure to MO (Yang *et al* 2014, Zhang *et al* 2020). On the other hand, the adsorption of BSA was related to its electrostatic interactions with the opposite charge sites on the surface of the PAC, TPAC, and CPAC samples, as explained earlier (Seredych *et al* 2018). According to pseudo-second-order reaction kinetics, the electrostatic forces between the adsorbate and adsorbent could significantly affect the electron exchange or sharing tendencies of the rate-limiting species in the solution, which may control the adsorption process (Li *et al* 2021). The rate of adsorption of BSA and MO due to surface exchange reactions may decrease due to the maximum surface coverage of the AC samples. Apart from the surface chemistry of AC, the porosity of carbonaceous material is an important factor in organic molecule adsorption. According to reports, the number of pores and BET surface area also correlate with the ability of smaller molecules such as MO and BSA to attach to the inner surface of carbon (Mojoudi *et al* 2019). Therefore, the adsorption of contaminants can be improved by applying ultrasonication, during which these molecules may diffuse into the porous structure of activated carbon through electrostatic interactions (hydrogen bonding). For instance, independent of the nature of the organic contaminant, the relatively large $q_{e,exp}$ values of TPAC compared to those of PAC and CPAC were associated with its high surface area and porous structure. Different activated carbon samples were found to adsorb these contaminants with similar kinetics, as per earlier results reported in the literature (Ma *et al* 2012, Seredych *et al* 2018, Hasani *et al* 2022).

### 3.4. Adsorption isotherms

The Langmuir and Freundlich models were used to investigate the adsorption behavior on the PAC samples using equations (6) and (7), respectively.

$$\frac{1}{q_e} = \frac{1}{K_e.q_{\max}}.\frac{1}{C_e} + \frac{1}{q_{\max}} \tag{6}$$

where $q_{\max}$ (mg/g) is the maximum monolayer adsorption capacity and $K_e$ (l/mg) is the Langmuir adsorption constant. $C_e$ is the concentration of the adsorbed contaminant measured experimentally.

$$\log q_e = \log K_f + \frac{1}{n}.\log C_e \tag{7}$$

$K_f$ and n represent the Freundlich adsorption constant and the heterogeneity factor, respectively. However, $1/n < 1$ conforms to the applicable adsorption processes. The Langmuir and Freundlich model parameters were determined to estimate the adsorption characteristics of the PAC samples for BSA and MO under the applied conditions. Figures S5(a), (b) shows the linear fitting of the $1/q_e$ versus $1/C_e$ (Langmuir) and $logq_e$ versus $logC_e$ (Freundlich) plots for MO adsorption over PAC samples during both batch and ultrasonication-assisted adsorption processes. Similarly, figures S5(c), (d) shows the adsorption isotherms of BSA on the PAC samples. A comparison between the Langmuir and Freundlich models revealed that the adsorption of BSA and MO well satisfied the Langmuir isotherm, as indicated by the linear fitting of the experimental data (Figures S5(a), (c)) and $R^2 > 0.9$ values (Iwuozor *et al* 2021). The corresponding $q_{\max}$, $K_e$, $1/n$, and $K_f$ values of PAC, TPAC, and CPAC for both BSA and MO are given in table S4. From the experimental data, it can be seen that the molecules of BSA

and MO were uniformly distributed on the surface of the PAC, TPAC, and CPAC samples following the Langmuir isotherm model (Xie *et al* 2020). Owing to the larger surface area and more porous structure of TPAC, its highest adsorption capacity for both BSA and MO can be justified. Furthermore, ultrasonication assisted the penetration of these contaminants within the porous structure of TPAC, resulting in a high adsorption capacity.

### 3.5. RSM modeling

#### *3.5.1. ANOVA for MO removal*

Analysis of variance (ANOVA) was used to evaluate the variance between the experimental parameters (time, initial concentration, and pH) and the modeling response of the CPAC under both conventional batch and ultrasonication conditions. The CPAC sample was chosen for RSM modeling due to its sensitivity to pH (see figure S2 in supplementary information). Equations (8), (9) show the relationships between the input parameters and response in terms of MO removal, which were determined through regression analysis. The contact time, initial concentration of adsorbate, and pH of the solution are represented by the variables (factors) A, B, and C, respectively, in these equations. Using these relationships, the main causes of performance variations, as well as the effects of each input variable on the response (removal efficiency of MO), were determined.

$$\begin{aligned} \%\ MO\ removal\ \text{by}\ CPAC\ (Unsonicated\ system) \ = \ & 85.8 + 7.3A - 10.5B - 6.1C - 0.75AB \\ & + 3AC + 0.25BC - 8.4A^2 + 1.2B^2 - 4.5C^2 \end{aligned} \tag{8}$$

$$\begin{aligned} \%\ MO\ removal\ \text{by}\ CPAC\ (Sonicated\ system) = \ & 91.9 + 6.8\,A - 6.6B - 6C - 0.87AB \\ & + 3.1AC - 0.37BC - 8.1A^2 + 1B^2 - 4.45C^2 \end{aligned} \tag{9}$$

Table S5 lists the input factors (contact time, initial concentration of MO and solution pH) and responses (% MO removal under both sonicated and unsonicated conditions) of 19 experimental runs for MO removal by the CPAC sample. Based on these findings, the F values of the model for MO obtained by batch adsorption and ultrasonication-assisted adsorption were 23.87 and 26.95, respectively, indicating the model's significance. This suggests that there is only a 0.01% chance that a large F value could occur due to noise. Furthermore, the significance of the model under investigation was corroborated by the extremely low P value of the model (P model for MO batch adsorption $<0.0001$ and MO ultrasonication-assisted adsorption $<0.0001$). This value also reflects the close agreement between the actual and predicted responses observed in figure S6 (*supplementary information*) (Khasawneh *et al* 2021). Additionally, the P values for both the linear and quadratic terms of the model were examined. In this analysis, the model terms A, B, C, and $A^2$ are significant (P value $< 0.05$), showing that time (A), initial concentration (B), pH (C), and a quadratic term are highly significant. In contrast, the remaining linear and quadratic terms of the model displayed lower levels of significance. Regression analysis was used to calculate the correlation coefficient ($R^2$) and to estimate the variability and accuracy of the developed models. The $R^2$ values, for instance, were 0.956 (without sonication) and 0.964 (with sonication) for the CPAC samples, as given in table S6 *(Supplementary information)*. Typically, $R^2$ values near 1 indicate a significant correlation between the predicted and observed values, indicating the accurate predictability of the model.

The effectiveness of the model was additionally confirmed and verified through a correlation plot comparing the predicted and actual values. Figure S6 Illustrates the linear relationship between the experimental (actual) and anticipated MO removal efficiencies for the CPAC sample. A diagnostic plot revealed a good connection between model predictions and observed values, demonstrating that the model provides a reliable assessment of the process under study (Gadekar and Ahammed 2019).

Figure S7 illustrates the combined effect of MO concentration and contact time on the percentage of MO removed. An increase in the MO concentration from 30 to 90 ppm reduced the removal efficiency from 54% to 40%. This indicates that with increasing MO concentration, the limited number of available active sites on CPAC became saturated. The adsorbed monolayer of the MO molecules frequently covers the external surface of the CPAC nanoparticles, which could subsequently reduce further adsorption. Figure S7(b) describes the combined effect of pH and MO concentration on MO removal efficiency based on the 3D plot, which shows that an increase in pH results in a decrease in MO removal efficiency at higher concentration values from 40 ppm to 70 ppm. As an anionic dye, MO has strong adsorption on the adsorbent surface due to the electrostatic attraction between its negative charges and the adsorbent (as the CPAC surface develops a positive charge in acidic media). As a result, MO is removed at a high rate under acidic conditions. In figure S7(c), the effectiveness of MO removal is shown as a function of contact time and pH. The contact time influences the contaminant removal efficiency because it affects the analyte mass transfer, which increases with extended contact. For instance, a maximum 93% removal efficiency was achieved in 45 min of contact time, and at a low pH of 5, the same removal efficiency could be achieved in approximately 25 min. Figures S7(d)–(f) shows the effect of initial concentration, pH, and time on the removal percentage of MO under ultrasonication conditions. The 3D graphs

in figures S7(d)–(f) follow the same trend as those shown in figures S7(a)–(c). However, relatively larger removal efficiencies were recorded due to ultrasonication, as discussed in the previous section (3.2.1).

*3.5.2. ANOVA for BSA removal*

The polynomial equations (10), (11) provides the relationships between the input variables and the percentage of BSA removed by CPAC, as determined via regression analysis. Using these equations, the main reasons for the variation in performance and the effect of the input variables on the % removal of BSA by CPAC can be predicted.

$$\%\ \text{BSA } \textit{removal} \text{ by } \textit{CPAC}(\textit{without sonication}) = 26.6 + 9.1A + 2.22B + 6.89C - 1.25AB - 0.25AC + 3BC - 1.81A^2 - 1.27B^2 - 1.1C^2 \quad (10)$$

$$\%\ \text{BSA } \textit{removal} \text{ by } \textit{CPAC}\ (\textit{with sonication}) = 36.08 + 12.79A + 3.11B + 9.55C - 1.8AB - 0.2AC + 4.2BC - 2.37A^2 - 1.88B^2 - 1.52C^2 \quad (11)$$

Table S7 lists the three input variables (factors) studied in 17 experimental runs and the % removal of BSA (response) by the CPAC sample. As given in table S8, the F values of the model for BSA by batch adsorption and ultrasonication-assisted adsorption were 10.95 and 11.25, respectively, indicating the model's significance. This suggests that there is only a 0.23% and 0.21% chance, respectively, that an F value this large could occur due to noise. Furthermore, the significance of the model under investigation was corroborated by the extremely low P value of the model (P model for BSA batch adsorption $<0.0023$ and for BSA ultrasonication-assisted adsorption $<0.0021$). This value also reflects the close agreement between the actual and predicted responses shown in figure 13 (Khasawneh *et al* 2021). Additionally, the P values for both the linear and quadratic terms of the model were examined. In this analysis, the model terms A and C are significant (for both batch and ultrasonication adsorption processes), showing that time (A) and pH (C) are highly significant. In contrast, the remaining linear and quadratic terms of the model displayed lower levels of significance. The correlation coefficient ($R^2$) was calculated using regression analysis, and its value reflected the precision of the developed models. For instance, the high $R^2$ values of 0.908 and 0.934 were attributed to the conventional batch (no sonication) and ultrasonication-assisted adsorption processes, respectively, suggesting the feasibility of the CCD model.

The predicted and experimental (actual) % removal of BSA by the CPAC samples were found to be linearly related to each other, as shown in figure S8 *(Supplementary information)*. The predicted and observed values for the experimental data have an excellent correlation $> 0.966$ for both processes (with and without sonication). Based on these diagnostic plots, a direct relation between the experimental and predicted responses validated the accuracy of the statistical modeling.

Figure S9(a) shows that increasing the BSA concentration from 30 to 90 ppm lowered the removal efficiency of CPAC. During the adsorption process, the availability of active sites on the CPAC sample initially promoted the abrupt adsorption of BSA. However, at high concentrations, after full surface coverage was achieved, further adsorption of protein molecules on CPAC was restricted. At high concentrations of BSA, adsorption is directly dependent on the total surface area of the CPAC and the availability of surface active sites (Stone and Kozlov 2014). As a result, after full surface coverage was achieved, a lower amount of BSA was subsequently adsorbed at high concentrations. Therefore, at high concentrations, CPAC saturation was achieved in less time. Figure S9(b) illustrates the combined effect of pH and BSA concentration on the % removal of BSA. The 3D contour plots demonstrate that the percentage of BSA removed increases with increasing pH at any fixed initial concentration of BSA. These results can be intuitively understood since positive charges often exist at pH levels below the isoelectric point of BSA (4.5–5.0), while negative charges typically exist at high pH levels. Consequently, at 3.0 pH, there is a stronger repulsion between positively charged BSA and CPAC, resulting in minimum adsorption (as discussed previously in section 3.2.2). The rate of BSA removal is affected by time and pH, as shown in figure S9(c). This is because contact time affects analyte mass transfer, which typically increases with increasing contact time and could impact the effectiveness of the contaminant removal process. The maximum adsorption (40%) occurred after 45 min of contact. Adsorption removal of BSA is low at a lower pH of 3 and a shorter contact time, while adsorption increases with time and increases with increasing solution pH. A study of the effect of initial concentration, pH, and duration on BSA removal with aided sonication can be found in figures S9(d)–(f). A similar pattern can be seen in all three 3D graphs in figures S9(d)–(f), although greater percentages of BSA removal were recorded due to the sonication effect.

*3.5.3. Optimization validation conditions for BSA and MO removal*

Table S9 (*Supplementary Information*) presents the optimal % removal of BSA and MO, as determined through RSM modeling. The verification run yielded results closely aligned with the predictions. Specifically, the actual BSA removal rate was 55%, with a percentage error of 4.1%, compared to the projected value of 51%. This indicates a 4% margin of error, which is deemed acceptable because it falls within the range of less than 5%.

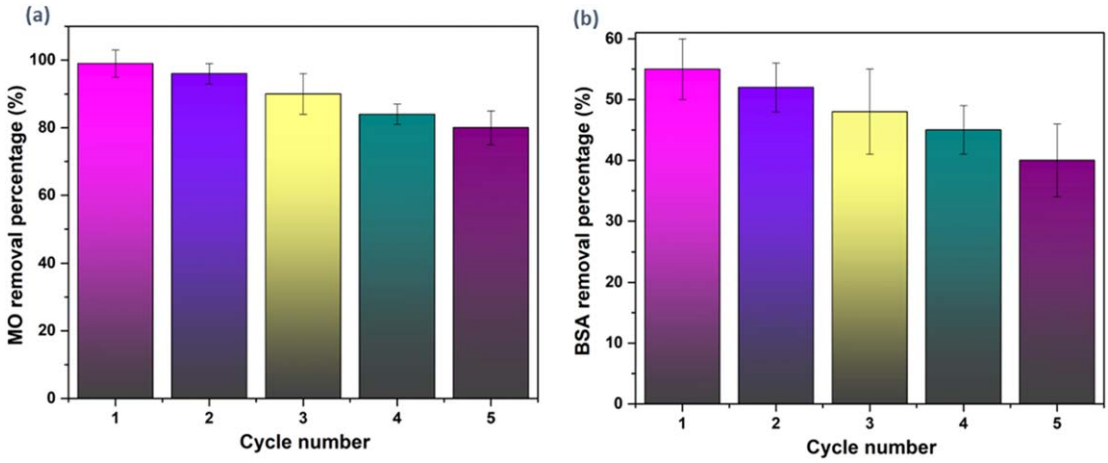


**Figure 7.** Effect of generation cycles of the removal of (a) MO and (b) BSA by the CPAC.

Additionally, the verification run for MO removal achieved an actual removal of 96%, with a mere 3% error from the projected value of 99%.

### 3.6. Cyclic adsorption/desorption, regeneration and post analysis

Adsorption and desorption experiments were conducted for five cycles, and the variations in adsorption capacity are illustrated in figure 7. With each successive regeneration, there was a slight decrease in the amount of adsorbed MO (from 98% to 80%) and BSA (from 55% to 40%). The decrease in the adsorption capacity of CPAC could be attributed to the deactivation of certain adsorption sites due to permanent chemical bonding, as described by 2nd-order kinetics of the adsorption process, and could also be due to a slight loss of adsorbent during the regeneration process (Altıntıg *et al* 2021).

The BET surface area for CPAC decreased significantly to 94 $m^2\ g^{-1}$ after the regeneration cycles. This reduction can be attributed to the partial collapse of the delicate pore structures of AC during chemical regeneration, which diminishes the available surface area for adsorption. Additionally, incomplete removal of adsorbed MO and BSA during regeneration may result in residual contaminants that occupy active sites, thereby reducing the surface area of AC. The SEM image (Figure S10) after the regeneration cycles reveals that the regeneration process for CPAC resulted in a dull appearance. The smoothening of edges observed is attributed to the repeated treatment with NaOH during regeneration process, which led to the etching of carbon, removing not only adsorbed materials but could also leach small amounts of the carbon itself.

Figure S11(a) shows the FTIR spectrum of CPAC after MO adsorption, highlighting a peak at 3437 $cm^{-1}$ attributed to N-H stretching (Wang *et al* 2020). Peaks at 1648 $cm^{-1}$ and 939 $cm^{-1}$ correspond to –C–H bending in aromatic rings and –C–H stretching vibrations of the benzene ring, respectively. The peak at 817 $cm^{-1}$ indicates –C–H stretching vibrations in a di-substituted benzene ring, confirming the aromatic nature of the dye. Peaks at 1361 $cm^{-1}$ and 1184 $cm^{-1}$ signify –C–N stretching, supporting the azo nature of the dye, while the peak at 1111 $cm^{-1}$ corresponds to –S=O stretching vibrations, confirming the sulfonic nature of MO (Cyril *et al* 2019).

Figure S11(b) presents the FTIR spectrum of BSA, showing the characteristic Amide-I band at 1654 $cm^{-1}$, typical of proteins with high $\alpha$-helix content. The band at 1545 $cm^{-1}$ is attributed to strong primary amine scissoring vibrations, while the peak centered at 3436 $cm^{-1}$ corresponds to primary amines. The band at 2959 $cm^{-1}$ is associated with C–H stretching vibrations, and the broad band at 702 $cm^{-1}$ is due to $–NH_2$ and –NH wagging (He *et al* 2013).The interaction between hydrogen atoms in the amine groups of CPAC and the oxygen atoms in MO and BSA is evident from the intensity of the peak around 3437 $cm^{-1}$ in the FTIR spectra of MO and BSA. This suggests effective adsorption facilitated by the chemical modifications of AC, as indicated by the changes observed in the spectra.

### 3.7. Comparative analysis

The data presented in table 1 illustrate findings from previous studies using various types of prepared and commercially available ACs. In comparison, the adsorption of MO using TPAC exhibited promising results compared to those of other previously employed adsorbents. The highest reported adsorption capacity in the literature was 113 mg $g^{-1}$ of MO using commercial AC. The highest adsorption capacity in this study was 152 mg $g^{-1}$ for MO and 133 mg $g^{-1}$ for BSA using TPAC with ultrasonication. Moreover, the adsorption

**Table 1.** A comparison of modified AC with other AC-based adsorbents in the literature under optimal conditions.

| Adsorbent | Adsorbate | Adsorption method | Adsorption capacity $q_{max}$ (mg/g) | Equilibrium time (min) | Removal percentage (%) | References |
|---|---|---|---|---|---|---|
| Commercial Activated Carbon | MO | Batch | 113 | 30 | 99 | (Khattabi *et al* 2021) |
| Nano activated carbon | MB | Batch | 28 | 90 | 98 | (Shokry *et al* 2019) |
| Commercial granular activated carbon | Azo dyes | Batch | 3.32 | 60 | 90–99 | (Khader *et al* 2021) |
| AC from orange peels | MO | | 33 | 40 | 96 | (Ramutshatsha-Makhwedzha *et al* 2022) |
| | | Batch | | | | |
| | MB | | 38 | 20 | 98 | |
| $TiO_2$ | BSA | Batch | 42.6 | 200 | No data | (Kopac *et al* 2008) |
| Hydroxyapatite NPs | BSA | Batch | 28 | 140 (h) | No data | (Swain and Sarkar 2013) |
| CPAC | MO | Batch, Ultrasonication | 126 | | 98 | This study |
| | | | | 60 | | |
| | | | 149 | | 99.5 | |
| | BSA | Batch, Ultrasonication | 100 | | 40 | |
| | | | | 60 | | |
| | | | 112 | | 57 | |
| TPAC | MO | Batch, Ultrasonication | 133 | | 98.5 | |
| | | | | 60 | | |
| | | | 152 | | 100 | |
| | BSA | Batch, Ultrasonication | 124 | | 63 | |
| | | | | 60 | | |
| | | | 133 | | 86 | |

capacities for MO and BSA using CPAC were also found to be quite significant, at 149 mg $g^{-1}$ and 111 mg $g^{-1}$, respectively. Thus, the modified ACs reported in this study are promising candidate adsorbents for the removal of MO and BSA organic pollutants.

### 3.8. Limitations and future prospects

This research was primarily conducted with two model pollutants under batch adsorption with and without sonication using RSM modeling. Future investigations should focus on studying the adsorption process of additional anionic dyes, cationic synthetic dyes, and their mixture using modified PAC to determine the effect of competing ions. Additionally, exploring the competition between organic molecules to occupy the available active sites of the adsorbent material would be beneficial at various pH values to better understand the interaction mechanism. Furthermore, future studies should focus on applying the findings from the present work to continuous flow systems under both dead-end and crossflow conditions by incorporating modified AC adsorbents in membranes for immobilization purposes. This approach could be used in real wastewater treatment systems by extending the results obtained from the pilot scale to a larger scale in practical field operations.

## 4. Conclusion

Thermal and chemical modifications of PAC were utilized to assess their adsorption capacities for removing BSA and MO from simulated wastewater. The impacts of PAC pretreatment, medium pH, initial contaminant concentration, contact time, and ultrasonication were examined to determine the adsorption capacities, kinetics, and mechanisms. The TPAC had a greater BET surface area of 823 $m^2 g^{-1}$ than did the CPAC (657 $m^2 g^{-1}$) due to the formation of a porous structure. The ultrasonication of the contaminated water improved the adsorption capacity of the PAC samples compared to the conventional batch adsorption process, as evidenced by the relatively large BSA and MO removal efficiencies. In the ultrasonication-assisted process, TPAC presented a $q_{max}$ of 152 mg $g^{-1}$ compared to PAC (124 mg $g^{-1}$) for MO in a batch adsorption process. Similarly, TPAC had a $q_{max}$ of 133 mg $g^{-1}$ for BSA compared to 112 mg $g^{-1}$ for PAC. Additionally, BSA and MO adsorption on CPAC was strongly influenced by the pH of the media due to electrostatic interactions, with MO favoring the highest removal at pH 3 and BSA at pH 5. The pseudo-second-order modeling analysis with $R^2 > 0.99$ revealed that the chemisorption of these contaminants controlled the adsorption kinetics. A comparison of Langmuir and Freundlich's isotherm modeling results suggested that the adsorption of MO and BSA progressed via the formation of a uniform monolayer on the PAC samples following the Langmuir adsorption model. For CPAC, the RSM analysis was performed using the CCD model to predict the optimized conditions for the highest removal efficiency of MO and BSA as a function of the input variables (i.e., pH, initial concentration, and contact time). The statistical analysis showed that with ultrasonication maximum removal is achieved for BSA at pH 5, initial BSA concentration of 60 ppm, and a contact time of 55 min) and for MO at pH 3, initial MO concentration of 45 ppm, and a contact time of 30 min. The regeneration test conducted on CPAC indicated limited reusability for up to five cycles for both the MO and BSA pollutants, with the efficiency remaining greater than 80% for MO. These results suggest that modified ACs are potential candidates for the enhanced and optimized removal of organic pollutants. This study serves as a valuable reference for optimizing and designing water treatment processes tailored to the textile and process industries.

## Acknowledgments

The authors wish to acknowledge the help and assistance of the Higher Education Commission of Pakistan (NRPU Project 6020), the Islamabad Research Directorate, and the Polymer Research Laboratory at the National University of Sciences and Technology for providing essential resources and analytical support.

## Data availability statement

All data that support the findings of this study are included within the article (and any supplementary files).

## Conflicts of competing interest

The authors declare that they have no known competing financial interests or personal relationships that could have appeared to influence the work reported in this paper.

## Credit authorship contribution statement

Conceptualization and methodology, IAK., MY; formal analysis, IAK, AUK.; investigation, and data curation, review and editing, EA, IAK, KMD; writing-original draft preparation, review, and editing, IAK, MY, RS, EA, KMD; supervision NMA; All authors have read and agreed to the publication of this manuscript.

## ORCID iDs

Kashif Mairaj Deen https://orcid.org/0000-0002-3619-2599
Muhammad Yasir https://orcid.org/0000-0001-8999-2779

## References

Abbas M A *et al* 2020 Surface modification of TFC-PA RO membrane by grafting hydrophilic ph switchable poly(acrylic acid) brushes *Adv. Polym. Technol.* **2020** 1–12
Abid Z, Abbas A, Mahmood A, Rana N F, Khan S J, Duclaux L, Deen K M and Ahmad N M 2022 Water treatment using high performance antifouling ultrafiltration polyether sulfone membranes incorporated with activated carbon *Polym.* (MDPI)
Adam M, Strubel P, Borchardt L, Althues H, Dörfler S and Kaskel S 2015a Trimodal hierarchical carbide-derived carbon monoliths from steam- and CO2-activated wood templates for high rate lithium sulfur batteries *J. Mater. Chem.* A **3** 24103–11
Adamczyk Z, Pomorska A, Nattich-Rak M, Wytrwal-Sarna M and Bernasik A 2018 Protein adsorption mechanisms at rough surfaces: serum albumin at a gold substrate *J. Colloid Interface Sci.* **530** 631–41
Al-Degs Y S, El-Barghouthi M I, El-Sheikh A H and Walker G M 2008 Effect of solution pH, ionic strength, and temperature on adsorption behavior of reactive dyes on activated carbon *Dye. Pigment.* **77** 16–23
Alharbi H A, Hameed B H, Alotaibi K D, Al-Oud S S and Al-Modaihsh A S 2023 Conversion of a mixture of date palm wastes to mesoporous activated carbon for efficient dye adsorption *Mater. Res. Express* **10** 015602
Altıntıg E, Yenigun M, Sarı A, Altundag H, Tuzen M and Saleh T A 2021 Facile synthesis of zinc oxide nanoparticles loaded activated carbon as an eco-friendly adsorbent for ultra-removal of malachite green from water *Environ. Technol. Innov.* **21** 101305
Attia A A, Rashwan W E and Khedr S A 2006 Capacity of activated carbon in the removal of acid dyes subsequent to its thermal treatment *Dye. Pigment.* **69** 128–36
Bal G and Thakur A 2021 Distinct approaches of removal of dyes from wastewater: a review *Mater. Today Proc.* **50** 1575–9
Bayer C 2010 The ecological impact of membrane-based extraction of phenolic compounds—a life cycle assessment study *Water Sci. Technol.* **62** 915–9
Beker U, Ganbold B, Dertli H and Gülbayir D D 2010 Adsorption of phenol by activated carbon: Influence of activation methods and solution pH *Energy Convers. Manag.* **51** 235–40
Bekhoukh A, Moulefera I, Zeggai F Z, Benyoucef A and Bachari K 2022 Anionic methyl orange removal from aqueous solutions by activated carbon reinforced conducting polyaniline as adsorbent: synthesis, characterization, adsorption behavior, regeneration and kinetics study *J. Polym. Environ.* **30** 886–95
Belayachi A, Bestani B, Bendraoua A, Benderdouche N and Duclaux L 2016 The influence of surface functionalization of activated carbon on dyes and metal ion removal from aqueous media *Desalin. Water Treat.* **57** 17557–69
Bonyadi Z, Kumar P S, Foroutan R, Kafaei R, Arfaeinia H, Farjadfard S and Ramavandi B 2019 Ultrasonic-assisted synthesis of Populus alba activated carbon for water defluorination: application for real wastewater *Korean J. Chem. Eng.* **36** 1595–603
Bui T S, Bansal P, Lee B K, Mahvelati-Shamsabadi T and Soltani T 2020 Facile fabrication of novel Ba-doped g-C3N4 photocatalyst with remarkably enhanced photocatalytic activity towards tetracycline elimination under visible-light irradiation *Appl. Surf. Sci.* **506** 144184
Bumajdad A and Hasila P 2023 Surface modification of date palm activated carbonaceous materials for heavy metal removal and $CO_2$ adsorption *Arab. J. Chem.* **16** 104403
Çalımlı M H, Demirbaş Ö, Aygün A, Alma M H, Nas M S, Khan A, Asiri A M and Şen F 2019 Equilibrium, kinetics and thermodynamics of bovine serum albumin from carbon based materials obtained from food wastes *Bionanoscience* **9** 692–701
Cyril N, George J B, Joseph L and Sylas V P 2019 Catalytic degradation of methyl orange and selective sensing of mercury ion in aqueous solutions using green synthesized silver nanoparticles from the seeds of derris trifoliata *J. Clust. Sci.* **30** 459–68
Danish M, Hashim R, Mohamad Ibrahim M N and Sulaiman O 2014 Response surface methodology approach for methyl orange dye removal using optimized Acacia mangium wood activated carbon *Wood Sci. Technol.* **48** 1085–105
De La Luz-Asunción M, Sánchez-Mendieta V, Martínez-Hernández A L, Castaño V M and Velasco-Santos C 2015 Adsorption of phenol from aqueous solutions by carbon nanomaterials of one and two dimensions: Kinetic and equilibrium studies *J. Nanomater.* **2015**
El-Bery H M, Saleh M, El-Gendy R A, Saleh M R and Thabet S M 2022 High adsorption capacity of phenol and methylene blue using activated carbon derived from lignocellulosic agriculture wastes *Sci. Rep.* **12** 1–17
El-Bindary M A, El-Desouky M G and El-Bindary A A 2022 Adsorption of industrial dye from aqueous solutions onto thermally treated green adsorbent: a complete batch system evaluation *J. Mol. Liq.* **346** 117082
Estrada A K, Cordova Lozano F and Lara Díaz R A 2021 Thermodynamics and kinetic studies for the adsorption process of methyl orange by magnetic activated carbons *Air, Soil Water Res.* **14** 1–11
Foo K Y and Hameed B H 2012 Textural porosity, surface chemistry and adsorptive properties of durian shell derived activated carbon prepared by microwave assisted NaOH activation *Chem. Eng. J.* **187** 53–62
Foo K Y and Hameed B H 2010 An overview of dye removal via activated carbon adsorption process *Desalin. Water Treat.* **19** 255–74
Gadekar M R and Ahammed M M 2019 Modelling dye removal by adsorption onto water treatment residuals using combined response surface methodology-arti fi cial neural network approach *J. Environ. Manage.* **231** 241–8
Geçgel Ü and Üner O 2018 Adsorption of bovine serum albumin onto activated carbon prepared from elaeagnus stone *Bull. Chem. Soc. Ethiop.* **32** 53–63

Gholami Derami H, Gupta P, Gupta R, Rathi P, Morrissey J J and Singamaneni S 2020 Palladium nanoparticle-decorated mesoporous polydopamine/bacterial nanocellulose as a catalytically active universal dye removal ultrafiltration membrane *ACS Appl. Nano Mater.* **3** 5437–48

Hamd A, Shaban M, Al-Senani G M, Alshabanat M N, Al-Ghamdi A, Dryaz A R, Ahmed S A, El-Sayed R and Soliman N K 2023 Comprehensive evaluation of zeolite/marine alga nanocomposite in the removal of waste dye from industrial wastewater *Sci. Rep.* **13** 1–17

Hamdaoui O and Naffrechoux E 2009 Adsorption kinetics of 4-chlorophenol onto granular activated carbon in the presence of high frequency ultrasound *Ultrason. Sonochem.* **16** 15–22

Hasani N, Selimi T, Mele A, Thaçi V, Halili J, Berisha A and Sadiku M 2022 Theoretical, equilibrium, kinetics and thermodynamic investigations of methylene blue adsorption onto lignite coal *Molecules* **27** 1856

He A, Lei B, Cheng C (S ), Li S, Ma L, Sun S and Zhao C 2013 Toward safe efficient and multifunctional 3D blood-contact adsorbents engineered by biopolymers/graphene oxide gels *RSC Adv.* **3** 22120–9

Ho Y S 2006 Review of second-order models for adsorption systems *J. Hazard. Mater.* **136** 681–9

Huang H, Yu J, Liu W and Jiang X 2015 Amino-functionalized multi-walled carbon nanotubes as novel adsorbents for selective adsorption of anionic dyes in aqueous solution *Nano* **10** 1–11

Iwuozor K O, Ighalo J O, Emenike E C, Ogunfowora L A and Igwegbe C A 2021 Adsorption of methyl orange: a review on adsorbent performance *Curr. Res. Green Sustain. Chem.* **4** 100179

Jawad A H and Abdulhameed A S 2020 Statistical modeling of methylene blue dye adsorption by high surface area mesoporous activated carbon from bamboo chip using KOH-assisted thermal activation *Energy, Ecol. Environ.* **5** 456–69

Jiang J, Gao Y, Pang S-Y, Lu X-T, Zhou Y, Ma J and Wang Q 2015 Understanding the role of manganese dioxide in the oxidation of phenolic compounds by aqueous permanganate *Environ. Sci. Technol.* **49** 520–8

Khader E H, Mohammed T J and Albayati T M 2021 Comparative performance between rice husk and granular activated carbon for the removal of azo tartrazine dye from aqueous solution *Desalin. Water Treat.* **229** 372–83

Khasawneh O F S, Palaniandy P, Palaniandy P, Ahmadipour M, Mohammadi H and Bin Hamdan M R 2021 Removal of acetaminophen using Fe2O3-TiO2nanocomposites by photocatalysis under simulated solar irradiation: Optimization study *J. Environ. Chem. Eng.* **9** 104921

Khattabi E H E, Rachdi Y, Bassam R, Mourid E H, Naimi Y, Alouani M E , and Belaaouad S 2021 Enhanced elimination of methyl orange and recycling of an eco-friendly adsorbent activated carbon from aqueous solution *Russ. J. Phys. Chem. B* **15** S149–59

Kopac T, Bozgeyik K and Yener J 2008 Effect of pH and temperature on the adsorption of bovine serum albumin onto titanium dioxide *Colloids Surf.* A **322** 19–28

Landi M, Naddeo V and Belgiorno V 2010 Influence of ultrasound on phenol removal by adsorption on granular activated carbon *Desalin. Water Treat.* **23** 181–6

Lekene R B N, Kouotou D, Ankoro N O, Kouoh A P M S, Ndi J N and Ketcha J M 2021 Development and tailoring of amino-functionalized activated carbon based Cucumerupsi manni Naudin seed shells for the removal of nitrate ions from aqueous solution *J. Saudi Chem. Soc.* **25** 101316

Lellis B, Fávaro-Polonio C Z, Pamphile J A and Polonio J C 2019 Effects of textile dyes on health and the environment and bioremediation potential of living organisms *Biotechnol. Res. Innov.* **3** 275–90

Li J, Huang L, Jiang X, Zhang L and Sun X 2021 Preparation and characterization of ternary Cu/$Cu_2O$/C composite: an extraordinary adsorbent for removing anionic organic dyes from water *Chem. Eng. J.* **404** 127091

Lima M de A, Andreou R, Charalampopoulos D and Chatzifragkou A 2021 Supercritical carbon dioxide extraction of phenolic compounds from potato (Solanum tuberosum) peels *Appl. Sci.* **11** 3410

Liu D, Zhang W, Lin H, Li Y, Lu H and Wang Y 2016 A green technology for the preparation of high capacitance rice husk-based activated carbon *J. Clean. Prod.* **112** 1190–8

Liu X, Tian J, Li Y, Sun N, Mi S, Xie Y and Chen Z 2019 Enhanced dyes adsorption from wastewater via $Fe_3O_4$ nanoparticles functionalized activated carbon *J. Hazard. Mater.* **373** 397–407

Lütke S F, Igansi A V, Pegoraro L, Dotto G L, Pinto L A A and Cadaval T R S 2019 Preparation of activated carbon from black wattle bark waste and its application for phenol adsorption *J. Environ. Chem. Eng.* **7** 103396

M-Ridha M J, Hussein S I, Alismaeel Z T, Atiya M A and Aziz G M 2020 Biodegradation of reactive dyes by some bacteria using response surface methodology as an optimization technique *Alexandria Eng. J.* **59** 3551–63

Ma J, Yu F, Zhou L, Jin L, Yang M, Luan J, Tang Y, Fan H, Yuan Z and Chen J 2012 Enhanced adsorptive removal of methyl orange and methylene blue from aqueous solution by alkali-activated multiwalled carbon nanotubes *ACS Appl. Mater. Interfaces* **4** 5749–60

Ma Y, Gao N, Chu W and Li C 2013 Removal of phenol by powdered activated carbon adsorption *Front. Environ. Sci. Eng.* **7** 158–65

Madondo N I and Chetty M 2022 Anaerobic co-digestion of sewage sludge and bio-based glycerol: optimisation of process variables using one-factor-at-a-time (OFAT) and Box-Behnken Design (BBD) techniques *South African J. Chem. Eng.* **40** 87–99

Meng L, Cho K-S and Park S-J 2009 $CO_2$ adsorption of amine functionalized activated carbons *Carbon Lett.* **10** 221–4

Mines P D, Thirion D, Uthuppu B, Hwang Y, Jakobsen M H, Andersen H R and Yavuz C T 2017 Covalent organic polymer functionalization of activated carbon surfaces through acyl chloride for environmental clean-up *Chem. Eng. J.* **309** 766–71

Mohammadi A A, Moghanlo S, Kazemi M S, Nazari S, Ghadiri S K, Saleh H N and Sillanpää M 2022 Comparative removal of hazardous cationic dyes by MOF-5 and modified graphene oxide *Sci. Rep.* **12** 1–12

Mojoudi N, Mirghaffari N, Soleimani M, Shariatmadari H, Belver C and Bedia J 2019 Phenol adsorption on high microporous activated carbons prepared from oily sludge: equilibrium, kinetic and thermodynamic studies *Sci. Rep.* **9** 1–12

Moosavi S, Lai C W, Gan S, Zamiri G, Akbarzadeh Pivehzhani O and Johan M R 2020 Application of efficient magnetic particles and activated carbon for dye removal from wastewater *ACS Omega* **5** 20684–97

Muniyasamy A, Sivaporul G, Gopinath A, Lakshmanan R, Altaee A, Achary A and Velayudhaperumal Chellam P 2020 Process development for the degradation of textile azo dyes (mono-, di-, poly-) by advanced oxidation process - Ozonation: Experimental & partial derivative modelling approach *J. Environ. Manage.* **265** 110397

Naushad M, Alqadami A A, AlOthman Z A, Alsohaimi I H, Algamdi M S and Aldawsari A M 2019 Adsorption kinetics, isotherm and reusability studies for the removal of cationic dye from aqueous medium using arginine modified activated carbon *J. Mol. Liq.* **293** 111442

Nifas G N G and Forteza R S 2019 Synthesis of activated carbon / chitosan composites and expanded graphite for symmetric supercapacitor *Journal of Material Sciences & Engineering* **8** 1–7

Ntakirutimana S, Tan W and Wang Y 2019 Enhanced surface activity of activated carbon by surfactants synergism *RSC Adv.* **9** 26519–31

Ohashi T, Jara A M T, Batista A C L, Franco L O, Lima M A B, Benachour M, Da Silva C A A and Campos-Takaki G M 2012 An improved method for removal of azo dye orange ii from textile effluent using albumin as sorbent *Molecules* **17** 14219–29

Panda H, Tiadi N, Mohanty M and Mohanty C R 2017 Studies on adsorption behavior of an industrial waste for removal of chromium from aqueous solution *South African J. Chem. Eng.* **23** 132–8

Qiu H, Lv L, Pan B C, Zhang Q J, Zhang W M and Zhang Q X 2009 Critical review in adsorption kinetic models *J. Zhejiang Univ. Sci.* A **10** 716–24

Ramutshatsha-Makhwedzha D, Mavhungu A, Moropeng M L and Mbaya R 2022 Activated carbon derived from waste orange and lemon peels for the adsorption of methyl orange and methylene blue dyes from wastewater *Heliyon* **8** e09930

Rondina D J G, Ymbong D V, Cadutdut M J M, Nalasa J R S, Paradero J B, Mabayo V I F and Arazo R O 2019 Utilization of a novel activated carbon adsorbent from press mud of sugarcane industry for the optimized removal of methyl orange dye in aqueous solution *Appl. Water Sci.* **9** 1–12

Sáenz-Alanís C A, García-Reyes R B, Soto-Regalado E and García-González A 2017 Phenol and methylene blue adsorption on heat-treated activated carbon: Characterization, kinetics, and equilibrium studies *Adsorpt. Sci. Technol.* **35** 789–805

Sakamoto M, Ahmed T, Begum S and Huq H 2019 Water pollution and the textile industry in bangladesh: flawed corporate practices or restrictive opportunities? *Sustain* **11** 1951

Seredych M, Mikhalovska L, Mikhalovsky S and Gogotsi Y 2018 Adsorption of bovine serum albumin on carbon-based materials *C* **4** 3

Shafeeyan M S, Daud W M A W, Houshmand A and Shamiri A 2010 A review on surface modification of activated carbon for carbon dioxide adsorption *J. Anal. Appl. Pyrolysis* **89** 143–51

Shokry H, Elkady M and Hamad H 2019 Nano activated carbon from industrial mine coal as adsorbents for removal of dye from simulated textile wastewater: Operational parameters and mechanism study *J. Mater. Res. Technol.* **8** 4477–88

Sivarajasekar N and Baskar R 2014 Adsorption of basic red 9 on activated waste Gossypium hirsutum seeds: process modeling, analysis and optimization using statistical design *J. Ind. Eng. Chem.* **20** 2699–709

Sk S and Aal F 2020 Advance research in textile engineering feasibility study on the reduction of phenol and chlorophenol concentration from the contaminated textiles using suitable detergent and dispersing agent *Adv. Res. Text. Eng.* **5** 01–6

Srivastava V C, Swamy M M, Mall I D, Prasad B and Mishra I M 2006 Adsorptive removal of phenol by bagasse fly ash and activated carbon: Equilibrium, kinetics and thermodynamics *Colloids Surf.* A **272** 89–104

Stone M T and Kozlov M 2014 Separating proteins with activated carbon *Langmuir* **30** 8046–55

Swain S K and Sarkar D 2013 Study of BSA protein adsorption/release on hydroxyapatite nanoparticles *Appl. Surf. Sci.* **286** 99–103

Szymaszek P, Fiedor P, Chachaj-Brekiesz A, Tyszka-Czochara M, Świergosz T and Ortyl J 2022 Molecular interactions of bovine serum albumin (BSA) with pyridine derivatives as candidates for non-covalent protein probes: a spectroscopic investigation *J. Mol. Liq.* **347** 118262

Tang K, Spiliotopoulou A, Chhetri R K, Ooi G T H, Kaarsholm K M S, Sundmark K, Florian B, Kragelund C, Bester K and Andersen H R 2019 Removal of pharmaceuticals, toxicity and natural fluorescence through the ozonation of biologically-treated hospital wastewater, with further polishing via a suspended biofilm *Chem. Eng. J.* **359** 321–30

Ünveren E E, Monkul B Ö, Sarıoğlan Ş, Karademir N and Alper E 2017a Solid amine sorbents for $CO_2$ capture by chemical adsorption: a review *Petroleum* **3** 37–50

Ünveren E E, Monkul B Ö, Sarıoğlan Ş, Karademir N and Alper E 2017b Solid amine sorbents for $CO_2$ capture by chemical adsorption: a review *Petroleum* **3** 37–50

Vukčević M M *et al* 2004 Phenol adsorption onto powdered and granular activated carbon, prepared from Eucalyptus wood *J. Colloid Interface Sci.* **279** 257–63

Wang C, Guo R, Lin S, Lan J, Jiang S and Xiang C 2018 A highly electro-conductive and flexible fabric functionalized with bovine serum albumin for a wearable electronic device *J. Mater. Sci., Mater. Electron.* **29** 14927–34

Wang G, Liu Y, Ye J, Lin Z and Yang X 2020 Electrochemical oxidation of methyl orange by a Magnéli phase $Ti_4O_7$ anode *Chemosphere* **241** 125084

Xie B, Qin J, Wang S, Li X, Sun H and Chen W 2020 Adsorption of Phenol on Commercial Activated Carbons: modelling and Interpretation *Int. J. Environ. Res. Public Health* **17** 1–13

Yang G, Chen H, Qin H and Feng Y 2014 Amination of activated carbon for enhancing phenol adsorption: effect of nitrogen-containing functional groups *Appl. Surf. Sci.* **293** 299–305

Yang J, Shojaei S and Shojaei S 2022 Removal of drug and dye from aqueous solutions by graphene oxide: adsorption studies and chemometrics methods *npj Clean Water* **5** 1–10

Yasir M, Asabuwa Ngwabebhoh F, Šopík T, Ali H and Sedlarík V 2022 Electrospun polyurethane nanofibers coated with polyaniline/polyvinyl alcohol as ultrafiltration membranes for the removal of ethinylestradiol hormone micropollutant from aqueous phase *J. Environ. Chem. Eng.* **10** 107811

Zhang Q, Cheng Y, Fang C, Chen J, Chen H, Li H and Yao Y 2020 Facile synthesis of porous carbon/$Fe_3O_4$ composites derived from waste cellulose acetate by one-step carbothermal method as a recyclable adsorbent for dyes *J. Mater. Res. Technol.* **9** 3384–93